Nuclear Mathematical and Computational Sciences: A Century in Review, A Century Anew
Gatlinburg, Tennessee, April 6-11, 2003, on CD-ROM, American Nuclear Society, LaGrange Park, IL (2003)

NONNEGATIVE ANISOTROPIC PIECEWISE-AVERAGE MULTIGROUP CROSS SECTIONS

David W. Gerts and Kirk A. Mathews*
Air Force Institute of Technology
AFIT/ENP, 2950 P Street -- Bldg 640, Wright-Patterson AFB, OH 45433-7765
David.Gerts@afit.edu; Kirk.Mathews@afit.edu

ABSTRACT

We present efficient, deterministic methods for obtaining piecewise-constant approximations for anisotropic group cross-sections, where the constant value in each interval of the cosine of the angle of scatter in the laboratory frame is the average in that interval. These averages are obtained by a combination of numerical and closed-form integrations of the ENDF/B-VI representations (ENDF laws and data files). Thus, the piecewise averages inherit the nonnegativity of the ENDF approximations. The resulting cross sections can be used directly for sampling scatter angles in multigroup Monte Carlo codes, or indirectly by producing equal-likelihood bins; they can be used to obtain discrete elements cross sections for discrete ordinates codes. This approach is new. It differs radically from the conventional approach that starts by expanding the group scattering cross sections in Legendre polynomials. These are often negative for some scattering angles and this is inevitable as energy groups are refined. Thus, they cannot be used directly to generate equal-likelihood bins for multi-group Monte Carlo calculations. Also, negative cross sections can lead to negative scattering sources in discrete ordinates calculations. These preclude the use of accurate, nonlinear, nonnegative spatial quadrature schemes such as the nonlinear exponential characteristic method and the nonlinear corner balance method. To generate equal-likelihood bins, current techniques attempt to reconstruct a positive function (an exponential of a Legendre polynomial) that matches the Legendre moments of the cross section. However, the coefficients cannot always be found except for relatively low-order approximations, and the exponential function introduces the artifact that the cross-section is strictly positive for all scattering angles if it is positive for any angles. Our approach eliminates all these difficulties.

Key Words: discrete elements ordinates exponential characteristic

1. INTRODUCTION

This work concerns the representation of, calculation of, and uses of the group-to-group cross section,

$$\sigma_{g',g}(\mu) \equiv \frac{\int_{E_{g'}}^{E_{g'-1}} dE' \, \Phi(E') \int_{E_g}^{E_{g-1}} dE \, \sigma(E' \to E, \mu)}{\int_{E_{g'}}^{E_{g'-1}} dE' \, \Phi(E')}, \tag{1}$$

where $\mu = \hat{\Omega}' \cdot \hat{\Omega}$ is the cosine of the scatter angle in the laboratory frame of reference and $\Phi(E')$ is an assumed-separable spectrum. Our tests used $\Phi(E') = 1/E'$. For simplicity of notation, we omit superscripts, subscripts and embellishments that would indicate material,

reaction, mechanism of that reaction, ENDF scattering law, or that would distinguish microscopic and macroscopic cross sections. We use $\int_{\Delta E_g}$ as an abbreviated form for $\int_{E_g}^{E_{g-1}}$.

We construct a piecewise average approximation and compare it with conventional cross sections. The range $[-1,1]$ is partitioned into *K* equal-width intervals,

$$\Delta\mu_k = \left[-1+2(k-1)/K, -1+2k/K\right]. \tag{2}$$

We also use the symbol to represent the size of the interval, $\Delta\mu_k = 2/K$; the meaning is clear from the context. The intervals need not be equal in width, but that choice is convenient so we have not yet implemented other choices. (A reason for a non-uniform mesh is discussed in section 3.2.) Then the piecewise-average cross section is

$$\sigma_{g',g}(\mu) = \bar{\sigma}_{k,g',g} \text{ for } \mu \in \Delta\mu_k , \tag{3}$$

where

$$\bar{\sigma}_{k,g',g} = \int_{\Delta\mu_k} \frac{d\mu}{\Delta\mu_k} \sigma_{g',g}(\mu) . \tag{4}$$

These cross sections provide efficient, deterministic calculation of discrete element cross sections for discrete ordinates transport and can be used for multigroup Monte Carlo transport.

2. MOTIVATION

Truncated Legendre series approximations to anisotropic group cross sections,

$$\sigma_{g',g}(\mu) \approx \sum_{\ell=0}^{L} (2\ell+1)\, \sigma^{\ell}_{g',g} P_\ell(\mu) , \tag{5}$$

use Legendre moments,

$$\sigma^{\ell}_{g',g} = \int_{-1}^{1} \frac{d\mu}{2} \sigma_{g',g}(\mu) P_\ell(\mu) , \tag{6}$$

that are computed from ENDF data by codes such as NJOY [1]. These are widely used in discrete ordinates calculations. However, they are typically not nonnegative, which creates difficulties in a number of ways. As we discuss in section 5, it can be impossible to avoid such negativities as resolution in energy is increased.

2.1. Nonnegative Fluxes in Discrete Ordinates Transport

In order to avoid negative ordinate-to-ordinate scattering cross sections in discrete ordinates transport calculations, DelGrande and Mathews [2] introduced discrete elements angular quadratures and their corresponding cross sections. Briefly, the sphere of direction of motion is

partitioned into elements of solid angle that do not overlap, but that collectively include all directions. (They tile the sphere.) The flux for element *n*, group *g* (also called bin *n*,*g*) is

$$\psi_{n,g} \equiv \int_{\Delta\Omega_n} d\Omega \int_{\Delta E_g} dE\, \psi(\Omega, E), \tag{7}$$

and the bin-to-bin cross section is

$$\sigma_{n',n,g',g} \equiv \frac{\int_{\Delta\Omega_{n'}} d\Omega' \int_{\Delta\Omega_n} d\Omega \int_{\Delta E_{g'}} dE' \,\Phi(E') \int_{\Delta E_g} dE\, \sigma\left(E' \to E, \hat{\Omega}' \cdot \hat{\Omega}\right)}{\Delta\Omega_{n'} \int_{\Delta E_{g'}} dE' \,\Phi(E')}. \tag{8}$$

With this approach, the linearized Boltzmann transport equation (discretized in direction and energy but not space) is

$$\bar{\Omega}_n \cdot \nabla \psi_{n,g} + \sigma_g \psi_{n,g} = Q^{ext}_{n,g} + \sum_{g'} \sum_{n'} \sigma_{n',n,g',g} \psi_{n',g'} \tag{9}$$

and nonnegativity of the cross sections and emission source ensure nonnegativity of the fluxes. Discretized in space as well, nonnegativity also requires a nonnegative spatial quadrature (spatial differencing) scheme, such as the nonlinear exponential characteristic [3] and nonlinear corner balance [4] methods.

DelGrande and Mathews used a Monte Carlo simulation to estimate these six-dimensional integrals. The practical limitations of that approach motivated this effort.

2.2. Avoiding Reconstruction of Nonnegative Cross Sections from Legendre Coefficients

In order to sample a direction of scatter from an anisotropic distribution in Monte Carlo transport calculations, it is first necessary to randomly choose the group *g* into which the particle is scattered. The groups are weighted by their conditional probabilities, given the group from which scattered:

$$P(g \mid g') = \frac{\int_{-1}^{1} d\mu\, \sigma_{g',g}(\mu)}{\sum_{g''} \int_{-1}^{1} d\mu\, \sigma_{g',g''}(\mu)} \tag{10}$$

Given the two groups, the cumulative distribution function (CDF)

$$F_{g',g}(\mu) = \frac{\int_{-1}^{\mu} d\mu'\, \sigma_{g',g}(\mu')}{\int_{-1}^{1} d\mu'\, \sigma_{g',g}(\mu')} \tag{11}$$

is approximated and inverted:

$$\mu_{sample} = F_{g',g}{}^{-1}(\xi), \tag{12}$$

where ξ is a pseudo-random number in the interval [0,1]. The approximation in equation 5, being a polynomial, is readily integrated to form the CDF, but if it is negative for some values of μ, the resulting cumulative function is not monotonic and so has no inverse. One way to avoid this is to construct a nonnegative function from the Legendre moments. The maximum entropy approximation [5] is

$$\sigma_{g',g}(\mu) \approx \exp\left[\sum_{\ell=0}^{L}(2\ell+1)\,\lambda_{\ell,g',g}P_\ell(\mu)\right], \tag{13}$$

where the coefficients λ are chosen so that the Legendre moments of the maximum entropy approximation equal (approximately) the (approximate) moments of the cross section. However, this root-finding or minimization problem is difficult and often intractable for *L* greater than about five. [5] The maximum entropy approximation is then used to produce a tabular approximation to *F*, for example, in the form of sixteen equal-likelihood intervals of μ.

Our piecewise-average cross sections avoid these intermediate approximations by directly providing a piecewise-linear CDF that can be inverted by table search and interpolation. We have used this technique successfully. [6] This CDF could then be used to construct equal-likelihood intervals in order to avoid the table search.

3. APPROACH

3.1. Scattering Operator

We define the scattering operator S,

$$\mathrm{S}_{g',g}\bullet \equiv \frac{\int_{-1}^{1} d\mu \int\limits_{\Delta E_{g'}} dE' \int\limits_{\Delta E_g} dE\, \sigma^s(E'\to E,\mu)\Phi(E')\bullet}{\int\limits_{\Delta E_{g'}} dE'\,\Phi(E')}, \tag{14}$$

where the dot is a placeholder for a function of μ. We use the scattering operators in three ways. The piecewise-average cross sections are

$$\bar{\sigma}_{k,g',g} = \mathrm{S}_{g',g}\,\frac{H(\mu_k-\mu)H(\mu-\mu_{k-1})}{\Delta\mu_k}, \tag{15}$$

where *H* is the Heaviside (unit step) function; the Legendre moments are

$$\sigma^{\ell}_{g',g} = \mathrm{S}_{g',g}\ P_{\ell}(\mu)/2\,; \tag{16}$$

and the discrete elements bin-to-bin cross sections are

$$\sigma_{n',n,g',g} = \mathrm{S}_{g',g}\ h_{n',n}(\mu)\,, \tag{17}$$

where $h_{n',n}(\mu)$ is the conditional probability of scattering from element n' to element n given that the incident direction is isotropically distributed in $\Delta\Omega_{n'}$ and that $\hat{\Omega}'\cdot\hat{\Omega} = \mu$. It is obtained by integrating a Dirac delta distribution over the elements:

$$h_{n',n}(\mu) = \int\limits_{\Delta\Omega_{n'}} \frac{d\Omega'}{\Delta\Omega_{n'}} \int\limits_{\Delta\Omega_{n}} d\Omega\ \delta\left(\hat{\Omega}'\cdot\hat{\Omega} - \mu\right). \tag{18}$$

Because a particle that scatters from element n' must scatter into some element n,

$$\sum_{n} h_{n',n}(\mu) = 1\,. \tag{19}$$

The nesting of integrals in equation 17 separates the calculation of discrete elements cross sections into two portions. The scattering operator captures the energy-mesh, spectrum, and material dependences; the conditional scattering probability encapsulates the geometric information of the discrete elements angular quadrature set. This formulation is the key to practical calculation of these cross sections. It also partitions the work into two tasks: (1) implementation of the scattering operator using nested deterministic numerical quadratures and ENDF/B-VI cross-section data and (2) numerical schemes for evaluating $h_{n',n}(\mu)$. This paper focuses on the first of these tasks.

3.2. Using Piecewise-Average Cross Sections to Obtain Discrete Element Cross Sections

Partitioning the integral with respect to μ in the S operator in equation 17 into pieces by introducing Heaviside functions yields

$$\sigma_{n',n,g',g} = \sum_{k=1}^{K} \mathrm{S}_{g',g}\ \frac{H(\mu_k - \mu)\,H(\mu - \mu_{k-1})}{\Delta\mu_k}\, h_{n',n}(\mu)\,\Delta\mu_k\,. \tag{20}$$

Next, within each piece, approximate $h_{n',n}(\mu)$ by its average value within the piece,

$$\overline{h}_{k,n',n} = \int\limits_{\Delta\mu_k} \frac{d\mu}{\Delta\mu_k}\, h_{n',n}(\mu)\,. \tag{21}$$

This constitutes a piecewise-average approximation to *h* that is exactly analogous to the piecewise-approximation to the cross section (on the same mesh in μ). Furthermore, because S is a linear operator and $h_{k,n',n}$ is a constant,

$$\mathrm{S}_{g',g}\,\frac{H(\mu_k-\mu)H(\mu-\mu_{k-1})}{\Delta\mu_k}\,h_{n',n}(\mu)\Delta\mu_k \approx \bar{h}_{k,n',n}\Delta\mu_k\;\mathrm{S}_{g',g}\,\frac{H(\mu_k-\mu)H(\mu-\mu_{k-1})}{\Delta\mu_k} \tag{22}$$

so that

$$\sigma_{n',n,g',g} \approx \sum_{k=1}^{K} \bar{h}_{k,n',n}\bar{\sigma}_{k,g',g}\Delta\mu_k\,. \tag{23}$$

This result is, in effect, a numerical quadrature for approximating

$$\sigma_{n',n,g',g} = \int_{-1}^{1} h_{n',n}(\mu)\,\sigma_{g',g}(\mu)\,d\mu\,, \tag{24}$$

that we call the composite product of means rule. It is analogous to the composite midpoint rule, with interval center values replaced by interval average values. For smooth functions $h(\mu)$ and $\sigma(\mu)$, the performance is quite similar, with $O(\Delta\mu^2)$ error. However, the product of means has advantages in this application.

Consider $\int_a^b f(x)g(x)dx$. If *f* and *g* are integrable, and *g* is nonnegative and finite in (*a*,*b*), then the integral exists and the integrand is bounded below by $f(x)g_{\min}$ and above by $f(x)g_{\max}$ where $g_{\min} = \min_{a\le x\le b}\left(g(x)\right)$ and $g_{\max} = \max_{a\le x\le b}\left(g(x)\right)$, so that

$$(b-a)g_{\min}\bar{f} \le \int_a^b f(x)g(x)dx \le (b-a)g_{\max}\bar{f} \tag{25}$$

where

$$\bar{f} = \int_a^b f(x)\frac{dx}{b-a}\,. \tag{26}$$

In our application, *h* is integrable and $0 \le h(\mu) \le 1$; while $\sigma(\mu)$ is nonnegative and integrable but may have one or more singularities. Equation 25 can be applied to every interval of the composite quadrature with *h* taking the role of *g*, or, in most intervals, with σ taking the role of *g*. This leads to the following bounds on the bin-to-bin cross section:

$$\sum_{k=1}^{K}\max\left(h^{\min}_{k,n',n}\bar{\sigma}_{k,g',g}, \bar{h}_{k,n',n}\sigma^{\min}_{k,g',g}\right)\Delta\mu_k \le \sigma_{n',n,g',g} \tag{27}$$

and

$$\sigma_{n',n,g',g} \le \sum_{k=1}^{K} \min\left(h^{\max}_{k,n',n}\overline{\sigma}_{k,g',g}, \overline{h}_{k,n',n}\sigma^{\max}_{k,g',g}\right)\Delta\mu_k \,. \tag{28}$$

The bounds converge to the cross section inversely with *K*, and can be used to select *K* large enough to guarantee a desired tolerance is met. It is also apparent that if $h(\mu)$ is slowly varying within each $\Delta\mu_k$, then the composite product of means approximation is useful despite large variations in $\sigma(\mu)$.

However, an unphysical result can be obtained where $\sigma_{g',g}(\mu)$ is zero in an interval within $\Delta\mu_k$ and positive elsewhere and $h_{n',n}(\mu) = 0$ wherever $\sigma_{g',g}(\mu) > 0$ and vice versa. In this case, $\int_{\Delta\mu_k} h_{n',n}(\mu)\sigma_{g',g}(\mu)\,d\mu = 0$ but $\overline{h}_{k,n',n}\overline{\sigma}_{k,g',g}\Delta\mu_k > 0$. This does occur. To demonstrate this, we examined the scattering cross sections for ${}^{1}_{1}H$, with $K = 64$, $G = 30$, and a one-dimensional 12-equal-element discrete element set (DE_{12}). This is an extremely challenging case, because each group scatters to itself and to all other lower-energy groups. Of the 66960 bin-to-bin cross sections, 12878 should have been zero, but 1390 of these were positive. The incorrectly positive bin-to-bin cross sections would be eliminated by using a non-uniform mesh such that $h_{n',n}(\mu)$ is either zero everywhere within $\Delta\mu_k$ or positive everywhere within $\Delta\mu_k$ for all element pairs and scattering cosine increments. For the DE_{12} set, 22 extra μ-mesh points are required to achieve this. This would require selection of a discrete element set (or sets) for which to construct the mesh.

For these hydrogen cross sections, the average relative difference between two calculation schemes, integration using a linear interpolation for $h_{n',n}(\mu)$ vs. piecewise averages, for the remaining cross sections was 3.8%. However, in view of equation 19, the piecewise average approach is superior: scatters from group to group are preserved exactly because

$$\begin{aligned}\sum_n \sigma_{n',n,g',g} &= \sum_k \overline{\sigma}_{k,g',g}\left(\sum_n \overline{h}_{k,n',n}\right)\Delta\mu_k \\ &= \sum_k \overline{\sigma}_{k,g',g}\Delta\mu_k \\ &= \int_{-1}^{1} \sigma_{g',g}(\mu)\,d\mu \,.\end{aligned} \tag{29}$$

Thus, the effect of the errors arising from the composite product of means rule is only a small increase in the numerical diffusion that the discretization in direction of motion inevitably entails.

4. IMPLEMENTATION OF THE SCATTERING OPERATORS

The ENDF laws can be grouped into classes by the form of dependence between E and μ. The form of the S operators for each of these classes is presented next.

4.1. ENDF/B-VI Energy and Scatter-Cosine Distributions

In general, ENDF/B-VI factors neutron cross sections as

$$\sigma\left(E' \to E, \mu\right) = \sigma\left(E'\right)\nu\left(E'\right) f_{joint}\left(\mu, E \mid E'\right), \tag{30}$$

where $\sigma\left(E'\right)$ is the microscopic cross section for the reaction/mechanism to occur for an incident neutron with kinetic energy E', $\nu\left(E'\right)$ is the expectation value of the number of secondary neutrons emitted given that the reaction/mechanism does occur, and $f_{joint}\left(\mu, E \mid E'\right)$ is the conditional joint probability density function for the distribution of the scattered neutron(s) in μ and E given that the incident neutron energy was E'. These scatter reactions, because of $\nu\left(E'\right)$, actually include fission, (n,2n) events, and so on.

The conditional joint probability density function is approximated in ENDF in a number of ways, called laws. The form of the joint distribution, of which there are four cases, determines the nesting of the integrations. In the separable class, in which μ and E are independently distributed, or are approximated as such,

$$f_{joint}\left(\mu, E \mid E'\right) = f\left(\mu \mid E'\right) g\left(E \mid E'\right), \tag{31}$$

the scattering operator is

$$S_{g',g}\bullet = \frac{\int\limits_{\Delta E_{g'}} dE'\,\sigma\left(E'\right)\nu\left(E'\right)\Phi\left(E'\right)\left(\int\limits_{-1}^{1} d\mu\, f\left(\mu \middle| E'\right)\bullet\right)\left(\int\limits_{\Delta E_g} dE\, g\left(E \middle| E'\right)\right)}{\int\limits_{\Delta E_{g'}} dE'\,\Phi\left(E'\right)}. \tag{32}$$

In the second class, the angular distribution is conditional upon the energy of the secondary,

$$f_{joint}\left(\mu, E \middle| E'\right) = g\left(E \middle| E'\right) f\left(\mu \middle| E', E\right), \tag{33}$$

and the scattering operator is

$$S_{g',g\bullet} = \frac{\int\limits_{\Delta E_{g'}} dE'\,\sigma(E')\nu(E')\Phi(E')\left(\int\limits_{\Delta E_g} dE\left(g(E|E')\int\limits_{-1}^{1} d\mu\, f(\mu|E',E)\bullet\right)\right)}{\int\limits_{\Delta E_{g'}} dE'\,\Phi(E')}. \tag{34}$$

In the third class, the energy of the secondary is conditional upon the scattering cosine,

$$f_{joint}(\mu, E|E') = f(\mu|E')\,g(E|E',\mu), \tag{35}$$

and the scattering operator is

$$S_{g',g\bullet} = \frac{\int\limits_{\Delta E_{g'}} dE'\,\sigma(E')\nu(E')\Phi(E')\int\limits_{-1}^{1} d\mu\left(f(\mu|E')\bullet\int\limits_{\Delta E_{g'}} dE\,g(E|E',\mu)\right)}{\int\limits_{\Delta E_{g'}} dE'\,\Phi(E')}. \tag{36}$$

The fourth class is a special case of the third class. It is specific to elastic and level-inelastic scatters. This case merits special treatment because elastic scatter occurs for all materials and all incident energy groups, and because each level of level-inelastic scatter is treated as another mechanism of scatter. Usually, most of the execution time of the program is spent calculating elastic and level-inelastic scatters. In these scatters, the scattering cosine and the secondary energy are deterministically related. This is expressed by a Dirac delta distribution for $g(E|E',\mu)$ in equation 35,

$$f_{joint}(\mu, E|E') = f(\mu|E')\,\delta(E - E_s(E',\mu)), \tag{37}$$

where E_s is determined by conservation of energy and momentum as

$$E_s(E',\mu) = \frac{1}{(A+1)^2}\left[\mu\sqrt{E'} \pm \sqrt{E'(\mu^2 + A^2 - 1) + A(A+1)Q}\right]^2, \tag{38}$$

where A is the ratio of the mass of the target nucleus to the mass of the neutron and Q is the kinetic energy of the product particles less that of the original particles. (Hence, when energy is absorbed in raising the target nucleus to an excited state, Q is negative.) For these scatters, the scattering operator is

$$S_{g',g}\bullet = \frac{\int_{\Delta E_{g'}} dE'\,\sigma(E')\nu(E')\Phi(E') \int_{\mu \ni E_g \le E \le E_{g-1}} d\mu f(\mu|E')\bullet}{\int_{\Delta E_{g'}} dE'\,\Phi(E')}. \quad (39)$$

The limits of integration with respect to μ are obtained from equation 38 by setting E_s to the energies that bound energy group *g*.

4.2. Reference Frames

The joint distribution data can be represented in ENDF/B-VI in either the center of mass reference frame or the laboratory reference frame. Where the ENDF/B-VI data is represented in the center of mass reference frame, then the scattering operators are transformed from the laboratory reference frame to the center of mass reference frame. Where the ENDF/B-VI data is represented in the laboratory reference frame, no transformation is required. Elastic and level-inelastic scatter distributions are well behaved in the center of mass frame, so the inner integral of the scattering operator in equation 39 is actually performed over the corresponding interval(s) in the center of mass (CM) frame. Let $\tilde{\mu}$ be the cosine of the scattering angle in the CM frame. ENDF provides data for $f(\tilde{\mu}|E')$, which is readily integrated. The transformation to the laboratory frame,

$$f(\mu|E') = f(\tilde{\mu}|E')\left|\frac{d\tilde{\mu}}{d\mu}\right| = \frac{f(\tilde{\mu}|E')}{\left|\frac{d\mu}{d\tilde{\mu}}\right|}, \quad (40)$$

is singular where $\frac{d\mu(\tilde{\mu})}{d\tilde{\mu}} = 0$. This condition is met for some scattering angle whenever the speed of the scattered particle in the CM frame is less than the speed of the center of mass measured in the lab frame. The algebra is rather ugly, so we present a physical argument: $\mu(\tilde{\mu})$ is continuous and differentiable. Exact backscatter in the CM frame is exact forward scatter in the lab frame, $\mu(\tilde{\mu}=-1)=+1$ while $0<\mu(\tilde{\mu}=0)<+1$, therefore $\left.\frac{d\mu(\tilde{\mu})}{d\tilde{\mu}}\right|_{-1} < 0$. But exact forward scatter in the CM frame is exact forward scatter in the lab frame, $\mu(\tilde{\mu}=+1)=+1$, so $\left.\frac{d\mu(\tilde{\mu})}{d\tilde{\mu}}\right|_{+1} > 0$. Therefore, there must be some intermediate value at which, $\frac{d\mu(\tilde{\mu})}{d\tilde{\mu}} = 0$. The geometry of this situation is that the scattered particle velocity in the lab frame (with a positive forward component) is perpendicular to the scattered particle velocity in the CM frame (with a backward component). This situation can arise in either of two ways. If the target nucleus is less massive than the neutron, e.g. ^1H, then this is the case even for elastic scatter. For all other nuclei, this applies only for inelastic collisions in which *Q* is large enough in magnitude. There are as many singularities as there are levels that meet this condition.

Because of these singularities, an interpolation of pointwise data for the cross section in the laboratory frame is impractical. The integration over μ in the scattering operators is essential for the success of our approach.

4.3. Numerical Quadratures

The choice of numerical quadratures is important to the efficiency of the code. Good choices are determined by the characteristics of the integrands. In each of the four classes, and for all the ENDF laws that we implemented, the integrands have some features in common.

- There are a finite number of discontinuities in the integrand.
- There are a finite number of discontinuities in its first derivative.
- There are a finite number of integrable singularities.
- The locations of the discontinuities and singularities are known or can be determined readily.

The discontinuities in value and in slope are treated by constructing a mesh in each variable that partitions the range of integration at each such discontinuity. In each interval of that mesh, a relatively low-order quadrature rule is usually appropriate because there is often little variability of the integrand within an interval. However, extra mesh refinement is needed in some intervals. To meet these needs, we use adaptive Simpson's-rule quadratures, implemented as Fortran-90 recursive functions. A user-set convergence criterion allows control over quadrature errors. In the vast majority of cases, an interval is subdivided only once, in effect, to confirm that the error tolerance is met. The adaptive scheme provides efficient mesh refinement in intervals that contain substantial, often localized, variation. Simpson's rule is appropriate because it reuses previously computed integrand points when the mesh is adaptively refined. However, where an endpoint of an interval is known to be the location of an integrable singularity, a 2-point Gauss-Legendre rule is used for the endmost subinterval instead, because it has the same order of accuracy as Simpson's rule but does not attempt to evaluate the integrand at the singularity. Other schemes could be devised and some might prove to be more efficient, but with these, the dominant computational cost is that of setting up the adaptive mesh to include all the points of bad behavior.

4.4. Doppler Broadening

We implemented Doppler broadening using methods developed for NJOY [1], but unlike NJOY, we use adaptive meshing to control error. Details are provided by Gerts [6].

5. EXAMPLE PIECEWISE-AVERAGE CROSS SECTIONS

We modified the LANL-30 group energy mesh [7] by replacing the top two groups (17-15 MeV and 15-13.5 MeV) with groups customized for problems in which the source of neutrons is D-T fusion (14.07 MeV): 14.1-14.0MeV and 14.0-13.5MeV. As energy resolution is increased, many

truncated Legendre expansions of $\sigma_{g',g}(\mu)$ are negative for some values of the scattering cosine. For example, the ^{10}B cross section for scatter from group 1 (14.1-14.0 MeV) to group 5 (10.0-7.79 MeV) is shown in figure 1. The piecewise-average cross-section for 64 intervals, marked PAX_{64} and drawn in bold, should be compared with the truncated expansions of orders P_0 through P_{11}, which are also shown on the plot. This example favors a high-order truncated Legendre expansion because the group-to-group cross section is strictly positive and, indeed, all expansions greater than P_4 are strictly positive.

On the other hand, when the cross section is exactly zero over a substantial range, a Gibbs phenomenon prevents high-order truncated expansions from being positive. Figure 2 shows the Boron cross section for scatter from group 1 to group 2. Only the P_0 approximation is nonnegative.

Even where usable high-order expansions are positive, as in figure 1, refining the energy groups can change that. For example, we split group 5 into four groups of equal width in lethargy. Figure 3 shows the PAX_{64} and P_{11} approximations for scatter from group 1 to the highest-energy group of the four subgroups of group 5. This example also demonstrates that as energy resolution is increased, higher angular resolution is needed — even P_{11} is insufficient to capture the shape that is revealed by the piecewise average cross sections.

It is also worth noting that the cross section in figure 3 has three regions of zero cross section, two of which are between regions of positive cross section. If 16 equal-likelihood bins are used for such cross sections, up to roughly 12% of the Monte Carlo draws would result in scatters that are not possible.

6. CONCLUSIONS

Actual group-to-group cross sections are often not smooth and have regions of zero value. Legendre expansions have long been used, perhaps because of the compactness of the data representation. However, it seems inappropriate to approximate C^0 functions with C^∞ basis functions. Unphysical negative cross section values are one result. The piecewise-average approximation used here eliminates the various artifacts and difficulties described in section 2.

Our nonnegative cross sections are an enabling technology — they make it possible to use advanced nonlinear, nonnegative spatial quadratures in discrete ordinates calculations with nonnegative anisotropic discrete element cross sections. This should remove one of the last barriers to their routine use in deterministic transport calculations. Together, these new techniques eliminate unphysical negative fluxes. It is our hope that this will increase acceptance of the discrete ordinates method by those who have never been comfortable with unphysical artifacts.

ACKNOWLEDGEMENTS

This work was conducted at the Air Force Institute of Technology as part of the official duties of the authors. Required disclaimer: The views expressed here are those of the authors and do not

reflect the official policy or position of the United States Air Force, Department of Defense, or the United States Government. This paper has been officially reviewed and assigned the following distribution notice: Cleared for Public Release — Distribution Unlimited.

REFERENCES

1. R. E. MacFarlane and D. W. Muir, "The NJOY Nuclear Data Processing System, Version 91", LA-12740-M, Los Alamos National Laboratory, (1994).
2. J. M. DelGrande and K. A. Mathews, "Nonnegative Anisotropic Group Cross Sections: A Hybrid Monte Carlo-Discrete Elements-Discrete Ordinates Approach", *Nuclear Science and Engineering*, **139**, pp. 33-46 (2001).
3. C. R. Brennan, R. L. Miller, and K. A. Mathews, "Split-Cell Exponential Characteristic Transport Method for Unstructured Tetrahedral Meshes," *Nuclear Science and Engineering*, **138**, 26 (2001). (See also its references.)
4. C. L. Castrianni and M. L. Adams, "A Nonlinear Corner-Balance Spatial Discretization for Transport on Arbitrary Grids," *Nuclear Science and Engineering*, **128**, pp. 278-296 (1998).
5. J. A. Dahl, "A Non-Linear Method for Representing the Scattering Cross Section for Discrete Ordinates," Joint Int. Conf. Mathematical Methods and Supercomputing for Nuclear Applications, Saratoga Springs, New York, October 6-10, 1997.
6. D. W. Gerts, "Efficient and Accurate Computation of Non-Negative Anisotropic Group Scattering Cross Sections for Discrete Ordinates and Monte Carlo Radiation Transport", Ph.D. Dissertation AFIT/DS/ENP/02-4, Air Force Institute of Technology (July 2002).
7. R. E. MacFarlane, "TRANSX 2: A Code for Interfacing MATXS Cross-Section Libraries to Nuclear Transport Codes", LA-12312-MS, Los Alamos National Laboratory (July 1992).

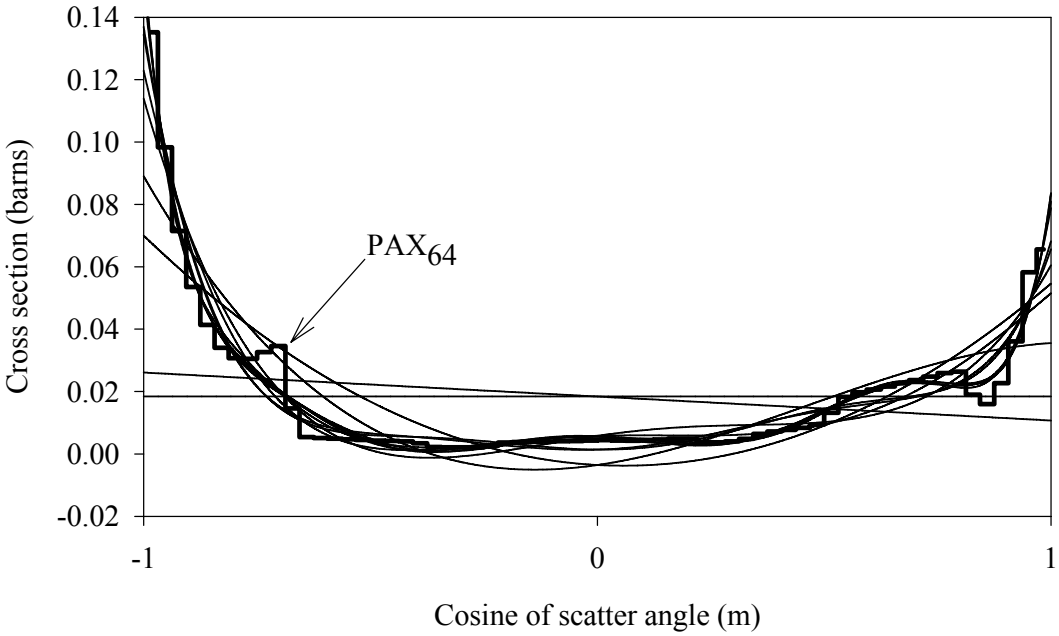

Figure 1: Negative regions for low order, L, for group 1 to group 5

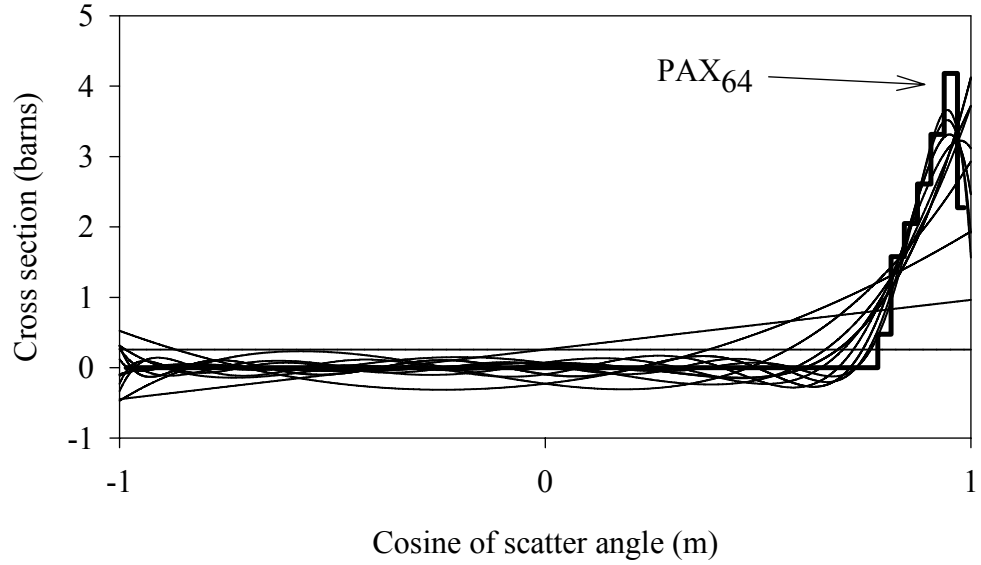

Figure 2: Negative regions for all L>0 for group 1 to group 2

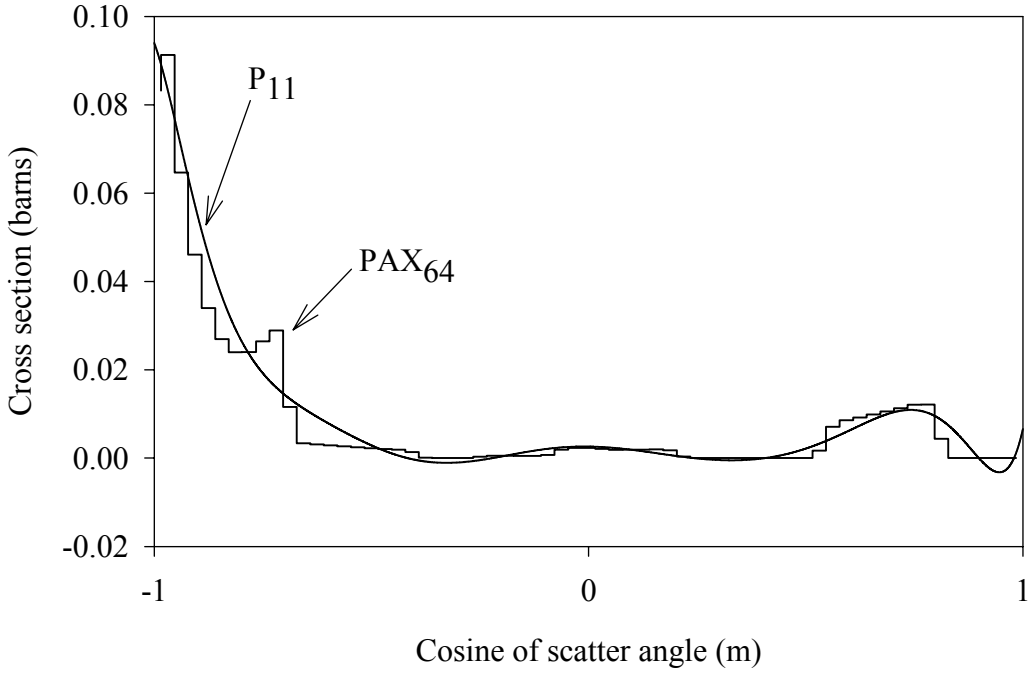

Figure 3: ^{10}B cross section for group 1 to upper fourth of group 5